Endothelial precursor cell-based therapy to target the pathologic angiogenesis and compensate tumor hypoxia

Guillaume Collet, Krzysztof Szade, Witold Nowak, Krzysztof Klimkiewicz, Bouchra El Hafny-Rahbi, Karol Szczepanek, Daisuke Sugiyama, Kazimierz Weglarczyk, Alexandra Foucault-Collet, Alan Guichard, et al.

Cancer Letters 370 (2016) 345–357

Contents lists available at ScienceDirect

Cancer Letters

journal homepage: www.elsevier.com/locate/canlet

Original Articles

Endothelial precursor cell-based therapy to target the pathologic angiogenesis and compensate tumor hypoxia

Guillaume Collet [a,b,1], Krzysztof Szade [a,b], Witold Nowak [a,b], Krzysztof Klimkiewicz [a,b], Bouchra El Hafny-Rahbi [a], Karol Szczepanek [a,b,2], Daisuke Sugiyama [c], Kazimierz Weglarczyk [a], Alexandra Foucault-Collet [a,1], Alan Guichard [a], Andrzej Mazan [a,b], Mahdi Nadim [a], Fabienne Fasani [a], Nathalie Lamerant-Fayel [a], Catherine Grillon [a], Stéphane Petoud [a], Jean-Claude Beloeil [a], Alicja Jozkowicz [b,d], Jozef Dulak [b,d,*], Claudine Kieda [a,d,**]

[a] Centre for Molecular Biophysics, Cell Recognition and Glycobiology, UPR4301-CNRS, rue Charles Sadron, Orléans 45071, France
[b] Faculty of Biochemistry, Biophysics and Biotechnology, Jagiellonian University, ul. Gronostajowa 7, Kraków 30387, Poland
[c] Division of Hematopoietic Stem Cells, Kyushu University Faculty of Medical Sciences, Maidashi, Higashi-Ku, Fukuoka 812-8582, Japan
[d] Malopolska Biotechnology Centre, Jagiellonian University, Gronostajowa 7A, Kraków 30387, Poland

ARTICLE INFO

Article history:
Received 6 October 2015
Received in revised form 4 November 2015
Accepted 4 November 2015

Keywords:
Endothelial precursor cells
Pathologic angiogenesis/vasculogenesis
Tumor targeting
Cell gene therapy

ABSTRACT

Hypoxia-inducing pathologies as cancer develop pathologic and inefficient angiogenesis which rules tumor facilitating microenvironment, a key target for therapy. As such, the putative ability of endothelial precursor cells (EPCs) to specifically home to hypoxic sites of neovascularization prompted to design optimized, site-specific, cell-mediated, drug-/gene-targeting approach. Thus, EPC lines were established from aorta–gonad–mesonephros (AGM) of murine 10.5 dpc and 11.5 dpc embryo when endothelial repertoire is completed. Lines representing early endothelial differentiation steps were selected: MAgEC10.5 and MagEC11.5. Distinct in maturation, they differently express VEGF receptors, VE-cadherin and chemokine/receptors. MAgEC11.5, more differentiated than MAgEC 10.5, displayed faster angiogenesis *in vitro*, different response to hypoxia and chemokines. Both MAgEC lines cooperated to tube-like formation with mature endothelial cells and invaded tumor spheroids through a vasculogenesis-like process. *In vivo*, both MAgEC-formed vessels established blood flow. Intravenously injected, both MAgECs invaded Matrigel™-plugs and targeted tumors. Here we show that EPCs (MAgEC11.5) target tumor angiogenesis and allow local overexpression of hypoxia-driven soluble VEGF-receptor2 enabling drastic tumor growth reduction. We propose that such EPCs, able to target tumor angiogenesis, could act as therapeutic gene vehicles to inhibit tumor growth by vessel normalization resulting from tumor hypoxia alleviation.

Introduction

Angiogenesis, the fundamental process of tissue vascularization, is induced by hypoxia in pathological contexts as cancer. Hypoxia occurs in the growing tumor and, to provide oxygen and nutrients to the tumor, angiogenesis proceeds by not only recruiting vicinal endothelial cells (ECs) but also circulating endothelial progenitor-like cells (EPCs) [1] thus achieving neo-vasculogenesis. Involved in tissue regeneration, these cells provide a potential therapeutic tool [2]. Despite controversies about the definition, characterization and classification of EPCs [3–6], cells presenting endothelial precursor features appeared to be involved in physiological and pathological processes in adults [7–12]. To clarify the definition, works about EPCs report the identification and characterization of new cell populations by describing increasingly complex EPC markers. They include VEGF receptors (VEGFR2, KDR, Flk-1), VE-cadherin, CD34, platelet endothelial cell adhesion molecule (PECAM; CD31), von Willebrand factor (VWF), the receptors for acetylated low-density lipoprotein (AcLDL) and for lectins as Bandeiraea simplicifolia-1 (BsA-1) and Ulex europaeus agglutinin-1 (UeA-1) [3,13–17].

* Corresponding author. Tel.: +48 12 664 63 75; fax: +48 12 664 69 18.
E-mail address: jozef.dulak@uj.edu.pl (J. Dulak).
** Corresponding author. Tel.: +33 238 25 55 61; fax: +33 238 25 54 59.
E-mail address: claudine.kieda@cnrs-orleans.fr (C. Kieda).
[1] Present address: Skaggs School of Pharmacy and Pharmaceutical Sciences, Laboratory of Bioresponsive Materials, University of California, San Diego, CA, USA.
[2] Present address: Metastasis Susceptibility Section, Laboratory of Cancer Biology and Genetics, Center for Cancer Research, National Cancer Institute, Bethesda, MD 20892, USA.

http://dx.doi.org/10.1016/j.canlet.2015.11.008

As such, EPCs have been found to be recruited and incorporated into neoangiogenic sites [18]; thus, they might participate to the proangiogenic effect of the bone marrow recruited cells and be well-suited tool to target pathologic sites [19]. The use of EPCs for therapeutic applications has been elaborated as a strategy to enhance endothelium regeneration [20–24], and EPCs were hypothesized to operate as vehicles to reach developing tumors for local therapies [25].

To study and optimize such strategies, an EPC model was needed. The use of well-defined and characterized cells was to provide a clear-cut answer to the question of tumor angiogenesis-mediated recruitment. In this line, such a well-defined EPC model should also be suitable as gene carrier to treat locally the tumor site via *in situ* incorporation in the vessels allowing the expression of the chosen gene in the local microenvironment.

In this purpose, we undertook to build a cell model of immature endothelial cells, characterize and define the best suited cell phenotype for tumor targeting and test their ability to express our previously described therapeutic gene for VEGF trap, i.e. the hypoxia-conditioned soluble receptor-2 for VEGF [26], which was shown to normalize the tumor vasculature. As the first cells committed to the endothelial lineage appear in aorta–gonad–mesonephros (AGM) [27,28], cells were isolated from this region at 10.5 and 11.5 days post conception (dpc), at which time cells diverge from the hemangioblast; the populations of the endothelial repertoire are potentially expressing the distinct degrees of endothelial maturation and are active, as described for hematopoietic cell production [29]. It has been reported that these cells express differentially CD34 [30], CD31, VEGFR2 (also known as Flk-1 and KDR) [31] and Tie-2 (also known as TEK and CD202) [32]. This total repertoire was expected for further establishment of cell lines allowing the determination of the proper phenotype of angiogenesis recruited EPCs.

Cell lines (patent pending) could be established; two of them were chosen as representing distinct endothelial differentiation steps at 10.5 dpc and 11.5 dpc. They were selected on the basis of their differentiation characteristics and called MAgECs (mouse aorta–gonad–mesonephros endothelial cells) 10.5 and 11.5. We used these lines to find out whether properly defined EPCs at precise differentiation step are able or not to target an angiogenic site. In such case, the present progress in induced pluripotent stem cell (iPS) [33] manipulation offers the potential to reach the proper EPC differentiation level [34] efficient for angiogenesis targeting [35]. iPS-derived EPCs can actively home in the tumor and metastasis sites, and upon genetic modification by a T cell costimulatory molecule, they reduce the numbers of metastatic sites as shown recently with CD40L-expressing cells [36].

We show here that the cell lines established from the AGM display endothelial precursor characteristics in terms of phenotype and angiogenic properties, depending on their maturation stage. Their potential to provide an effective cell model of EPC *in vivo* is proven by their ability to reach neoangiogenic sites and to cooperate with mature endothelial cells in the formation of angiogenesis functional network, thus participating to normal neovessel formation inside the tumor. Moreover, isolated, immortalized and characterized, endothelial precursor cell lines permitted to establish the proof of concept that an efficient cell-mediated gene therapy can be achieved with EPCs as vehicles. This is demonstrated in this work with MAgECs carrying a hypoxia-conditioned therapeutic gene which were able to target a tumor and reduce its growth. We show that gene therapy can be addressed by defined EPCs to hypoxia-developing diseases which, as cancer, set pathologic angiogenesis for their development. Differing from VEGF traps, this method brings the means to get a natural cell-mediated targeting of hypoxia-conditioned and reversible msVEGFR2 gene expression. It may meet the challenge of alleviating hypoxia instead of starving tumors to potentiate new anti-tumor strategies [37,38].

Materials and methods

Ethics statement

All animal related experiments were conducted in accordance with the approved guidelines and regulations. Experimental protocols were approved by the French Ethics Committee for Animal Experimentation CNRS Orleans Campus CNREEA 03 Ethics Committee, authorization number CLE CCO 2010-004.

Isolation of mouse aorta–gonad–mesonephros embryonic cells (MAgECs)

Animal care and experimental procedures were approved by the CNREEA 03 Ethics Committee. Embryos were taken from 10.5 dpc and 11.5 dpc pregnant FVB mice (TAAM CNRS, Orléans). Aorta–gonad–mesonephros (AGM) regions were isolated and washed extremely gently in RPMI (Gibco Invitrogen) supplemented with FBS 15% (PAA, Austria) and 40 µg/mL gentamicin (Gibco Invitrogen). Then the AGM derived tissues were cut into very small pieces and cell cultures were started at 37 °C in a 5% CO_2/95% air atmosphere in plastic culture plates (Falcon, Becton Dickinson, USA) using OptiMEM (Gibco Invitrogen) supplemented with 2% FBS, 40 µg/mL gentamicin (Gibco Invitrogen) and 0.5 µg/mL fungizone (Gibco Invitrogen). Cells were further immortalized and cultured as indicated in the Supplementary methods.

Cell culture in hypoxia

Cells were placed in a humidified atmosphere containing 1% oxygen. This controlled oxygen pressure was obtained by introducing 95% N_2/5% CO_2 gas mixture (Air Liquide, Paris, France) in an automated PROOX *in vitro* chamber (C-174, BioSpherix) under the control of a PROOX sensor-model 110 (BioSpherix). For larger scale culture and spheroid settings, hypoxia was established in the H35 HypOxystation (HypOxygen) using the various substrates and the media were kept for at least 10 h in hypoxia before use to enable the equilibrium between liquids and the atmosphere.

Quantitative PCR

Extraction of cellular mRNA was performed using the RNeasy Plus mini kit (Qiagen) according to the manufacturer's instructions. The hypoxia stimulation of MAgECs 10.5 and 11.5 was stopped after 24 hours with RNA isolation. All extracted mRNAs were eluted in RNase-free water. Absorption spectra were measured on an ND-1000 spectrophotometer (NanoDrop Technologies, Wilmington, DE) before being stored at –80 °C. RNAs were reverse-transcribed to cDNA using "Maxima First Strand cDNA Synthesis kit for RT-qPCR" (Fermentas). All reactions were completed in triplicate and reported as the average. For reference, 7 housekeeping genes were tested. Mean and standard deviation were calculated and the gene which had the lowest standard deviation was chosen for reference. For each target gene, mean and standard deviation were calculated by cell line (10.5 or 11.5) and condition (normoxia or hypoxia), then normalized by the corresponding value for reference gene (PPIA) to obtain the ΔCp which is expressed as $2^{-\Delta Ct}$. In the second step, the same method was used to compare hypoxia to normoxia and obtain the ΔΔCp.

Characterization at the protein expression level was assessed by immunochemistry, cytometry, and ELISA (Supplementary methods).

In vitro *pseudo tube formation assay*

Pseudo tube formation was performed on 96-well plates coated with 50 µL of Matrigel™ (BD Biosciences, San José, CA) diluted at ½ in OptiMEM. After polymerization at 37 °C, 8×10^3 cells/well were seeded in OptiMEM and the plate was introduced into the incubation chamber of the video microscope station. Controlled time-lapse acquisitions each 30 minutes were performed over 24 h with a Zeiss Axiovert 200M fluorescence inverted microscope (Zeiss) equipped with an Axiocam high-resolution numeric camera linked to a computer driving the acquisition software Axiovision (Zeiss). Tube-like and network structures were documented after 12 hours of culture. Each MAgEC cell line was studied independently and mixed together with mature endothelial cells to study hybrid angiogenesis.

In vivo *vascularization*

All animal experiments were approved by the CNREEA 03 Ethics Committee. 8 to 10-week-old female C57Bl/6 mice (Janvier S.A.S, Le Genest-St-Isle, France) were used for the studies. Mice were anesthetized by 2.5 vol % isoflurane (Aerrane®, Maurepas, France)/air mixture injected at 2 L/min. After site disinfection with 70% ethanol, 250 µL of Matrigel™ (BD Biosciences, Matrigel matrix phenol red free, 356237) supplemented with 500 ng/mL bFGF (R&D Systems) was mixed with cell culture medium (OptiMEM) 1:1 vol containing 10^5 cells, MAgEC 10.5 or MAgEC 11.5. The mixture was introduced subcutaneously in the abdominal region using a 21-gauge needle. Control was a cell free plug bearing mouse. Matrigel plug was imaged 10 days after by ultrasound imaging, macroscopic evaluation of vessel structures and surgical removal. 100 µL of a TRITC–dextran (MW 2,000,000, FD2000S, Sigma) solution at 10 mg/mL in saline was intravenously injected in the tail vein for angiogenesis visualization using a Nikon AZ100 Multizoom, equipped with an EMCCD Evolve 512 photometric camera and driven by the Nikon NIS Element BR software.

Acquisitions were done on reversed skin of the sacrificed mice. For epi fluorescence imaging Intensilight HGFIE HG, pre-centered fiber illuminator (130 W mercury) was used. Fluorescence channels filter (Semrock, Rochester, New York, USA) combinations for FITC: λ_{ex} 482/35 nm, beam splitter 506 nm, λ_{em} 536/40 nm; for TRITC: λ_{ex} 543/22 nm, beam splitter 562 nm, λ_{em} LP561 nm.

Ultrasound imaging

Plug images were acquired using a VisualSonics Vevo® 2100 Imaging System (VisualSonics Inc., Toronto, Ontario, Canada) connected to MS500D ultrasound transducers (22–55 MHz). Before imaging, the region of interest was depilated by a cream (Veet). Imaging was performed under anesthesia. A medical ultrasound acoustic gel was used as a coupling fluid between the transducer and the skin. Biological parameters were constantly monitored with the VisualSonics integrated rail system with physiological monitoring unit to assess the electrocardiograms (ECGs) of the animals and respiratory rate. Body temperature was maintained at 37.5 °C.

Ultrasound imaging was performed with B-mode to locate the Matrigel™ plug and to position the transducer perpendicularly to the body. Then blood flow (vein and artery) was measured using color Doppler mode and fitting it with B-mode imaging.

The imaging was driven and computed with VisualSonics Vevo® 2100 software.

GFP⁺ MAgEC cell line establishment

Both MAgEC cells, 10.5 and 11.5, were transfected with a GFP coding vector (pdAAV-CMV-GFP, 4994 bp, J. Stepniewski). Transfections were performed using the jetPEI™ (Polyplus Transfection, France) as DNA complexing agent according to the manufacturer's instructions with the ratio: 1 μg DNA/1 μL of jet-PEI solution. After recovery, transfected cells were cloned by a MoFlo™ cell sorter (MoFlo™, Beckman Coulter, Miami, FL, USA). The higher stably GFP expressing clones, for each MAgECs 10.5 and 11.5, were selected and expanded.

In vivo *MAgEC recruitment at angiogenic sites*

To assess the recruitment of MAgEC cells to newly forming blood vessels, a neoangiogenic site was induced by Matrigel plug into adult female C57Bl/6 mice (6–8 weeks old) (Janvier, France). Briefly, 500 μL of Matrigel containing 500 ng/mL VEGF + bFGF was implanted by subcutaneous injection in the abdominal region. After Matrigel polymerization, 2×10^6 GFP⁺-MAgECs 10.5 and 11.5 into 100 μL of saline were intravenously injected in the tail vein. After 10 days following the GFP⁺-MAgEC injection, the mice were sacrificed and peripheral blood was collected by cardiac punction with citrate syringe (citrate-dextrose solution, Sigma, C3821). After RBC lysis, single-cell suspensions were filtered using a 70 μm cell strainer (BD Falcon, 352350) just before flow cytometer analysis. Single cell suspensions were prepared from the plugs, lungs, and bone marrows by collagenase digestion of 1–3 mm^3 fragments (1.0 mg/mL (Invitrogen) in PBS–FBS 10% for 2 hours at 37 °C). Then, cells were filtered using the 70 μm cell strainer (BD Falcon, 352350) and washed twice before analysis and analyzed with a BD LSR-I flow cytometer (Becton and Dickinson). The proportion of GFP⁺ cells was investigated in each sample collecting 10^6 events. For histochemistry plugs were analyzed at day 7 after MAgEC injection.

MAgEC transfection by msVEGFR2 hypoxia dependent gene expressing vector

Vectors (pHREmsVEGFR2, pIFP1.4-HREmsVEGFR2, and IFP1.4_pcDNA3.1H.ape) were introduced into MAgECs to establish stable cell lines as described [26] by the cationic lipid "lipofectin" and "lipofectamine" (Invitrogen, Carlsbad, CA) methods. Transfected cells were selected by hygromycin, and resistant colonies were single-cell cloned by a FACS DIVA cell sorter (Becton and Dickinson, Sunnyvale, USA) and expanded. Clones were screened on the basis of their msVEGFR2 secretion in hypoxia (1% O_2) using ELISA method (R&D DY1558B).

MAgECs targeting of tumors and therapeutic gene expression

Transfected MAgEC clones were selected on the basis of msVEGFR2 expression in hypoxia (Supplementary results), were DiD-labeled and were used to be i.v. injected (10^6) to B16 tumor carrying mice, 9 days after tumor development (10^4 B16 cells per mouse). After 7 days the various organs and the tumors were isolated, weighed and analyzed for the MAgEC cell content by flow cytometry analysis on the FACS DiVa flow cytometer (Becton and Dickinson). As representative, statistical data were collected upon accumulation of 10^6 cells. Controls were obtained upon similar injection of PFA (3%)-fixed DiD-labeled MAgEC cells and MAgEC cells carrying the msVEGFR2 expression vector.

Spheroid formation

Spheroids were generated as described by Korff et al. [39]. From trypsinized confluent monolayer, 10^6 cells were labeled with 5 μL of the fluorescent Vybrant® Dye (Life Technologies, V-22889) in 1 mL of serum free medium and incubated 10 minutes at 37 °C. Then 1000 B16F10 cells were mixed with 0.25% (w/v) methylcellulose (Sigma) solution in culture medium (100 μL) and seeded in non-tissue culture treated 96-well plate V-shaped (Nunc, 277143). After 48 h of incubation at 37 °C in a 5% CO_2/95% air atmosphere, a single spheroid per well was obtained. Where noticed, to mimic tumor angiogenesis the fluorescent tumor cells were mixed in a 100/1 ratio with mature endothelial cells (MLuMEC) to form the spheroids.

For further introduction into a 3D matrix, spheroids were taken from the 96-well plate, washed by sedimentation, and mixed with non-polymerized collagen-based matrix together with the additional cells for further study. The matrix composition was: 1.6 mg/mL collagen type I (BD Biosciences, rat tail high concentration, 354249), 1.12% of methylcellulose (R&D System, HSC001) and 10% SVF. In a 1.5 cm diameter well, 225 μL of the matrix mixed with 30 spheroids and 10^5 Vybrant Dye labeled MAgEC10.5 or MAgEC11.5 or MLuMECs cells was deposited. After matrix polymerization at 37 °C, the plate was introduced into the incubation chamber of the video Zeiss Axio Observer Z1 fluorescence inverted microscope (Zeiss) equipped with an ORCA-R2 high-resolution CCD camera linked to a computer driven-acquisition software Axiovision (Zeiss) to control time-lapse acquisitions (30 min) over 24 h.

Cell recruitment toward spheroids was analyzed with the RG2B colocalization plug in with the NIH ImageJ software. Integrated density of colocalized pixels is used for the analysis.

Magnetic resonance imaging

10 days before the imaging, mice were injected subcutaneously with 5×10^5 B16F10 *wt* melanoma in 0.9% NaCl (w/v) in 10×10^6 cells/mL and mixed 1:1 (v:v) with Matrigel before the injection.

For magnetic resonance imaging, cells were labeled with Anionic Magnetic NanoParticles (AMNP) kindly provided by Dr Florence Gazeau (MSC laboratory, CNRS/University Paris Diderot, Paris France). After rinsing with OptiMEM, 5 mM sodium citrate containing 2 mM AMNP was added and cells were incubated in 37 °C, 5% CO_2 for 15–20 minutes, then the medium was changed to complete OptiMEM. Cells were used for intravenous injections 24 h after labeling at a 10×10^6 cells/mL concentration. 100 μL of cell suspension was injected intravenously to B16F10 tumor harboring mice. Control were mice injected with 1×10^6 4% PFA killed labeled MAgEC11.5 and mice injected with 100 μL of 0.9% NaCl (w/v). Mice were imaged with Bruker BioSpin 9.4 T spectroscope before and 24 h after the intravenous injections.

MR experiments were performed on an imaging spectrometer equipped with a 9.4 T horizontal shielded magnet (94/20 Ultra Shielded Refrigerated (USR), Bruker Biospec), a B-G06 gradient system (950 mT/m maximum gradient strength and 60 mm inner diameter), a BLAH1000 RF power amplifier and the Paravision 4.0 software (Bruker Biospin MRI, Wissembourg, France). The anesthetized mice were placed in a linear homogeneous coil (inner diameter: 35 mm) under gaseous anesthesia during MRI experiments (50% N_2O, 0.7 L/min–50% O_2, 0.7 L/min–isoflurane, 1.5%). The body temperature (36 °C) was maintained constant by a warm water circulation heating bed. Breathing rate was monitored by an air pillow placed on the mouse chest to adjust the anesthetic output.

FLASH pulse sequence was used. Total duration: 12 min, NS = 4, 63 axial slices were acquired (slice thickness: 0.5 mm), FOV: 3.0 × 3.0 cm, 256 × 256 matrix, resolution: 117 × 117 μm, TE = 4.34 ms, TR = 700 ms, Hermitian pulse (1.0 ms).

Results

Establishment of immortalized cell lines from AGM region of murine 10.5 dpc and 11.5 dpc embryos

From the AGM region of murine 10.5 and 11.5 dpc embryos, we immortalized as described and obtained many cloned cell lines. Two representative lines were selected and called MAgEC 10.5 and MAgEC 11.5 respectively. Their doubling time was approximately 24 hours. As reported in Fig. 1A, their morphologies were different. MAgEC 10.5 displayed a more dendritic/mesenchymal aspect than MAgEC 11.5 cells which were less elongated and had square shapes. Confluence was reached at a cell density close to 8×10^4 cells/cm^2 when MAgEC 10.5 take a more cobblestone-like aspect than at weaker concentration (Fig. 1A).

MAgECs 10.5 and 11.5 express endothelial stem cell markers and angiogenesis regulation factors

Immortalized cells (Fig. 1A) were extensively characterized for stem (Fig. 1B), endothelial (Fig. 1B, C) and mesenchymal markers (Fig. 1B). MAgECs are both highly expressing the Sca-1 stem cell marker and the CD34 as well. CD133 was not expressed on any of the lines. Mesenchymal stem cell combination of markers CD90 and CD105 was detected and CD29 and CD49e integrins were highly expressed.

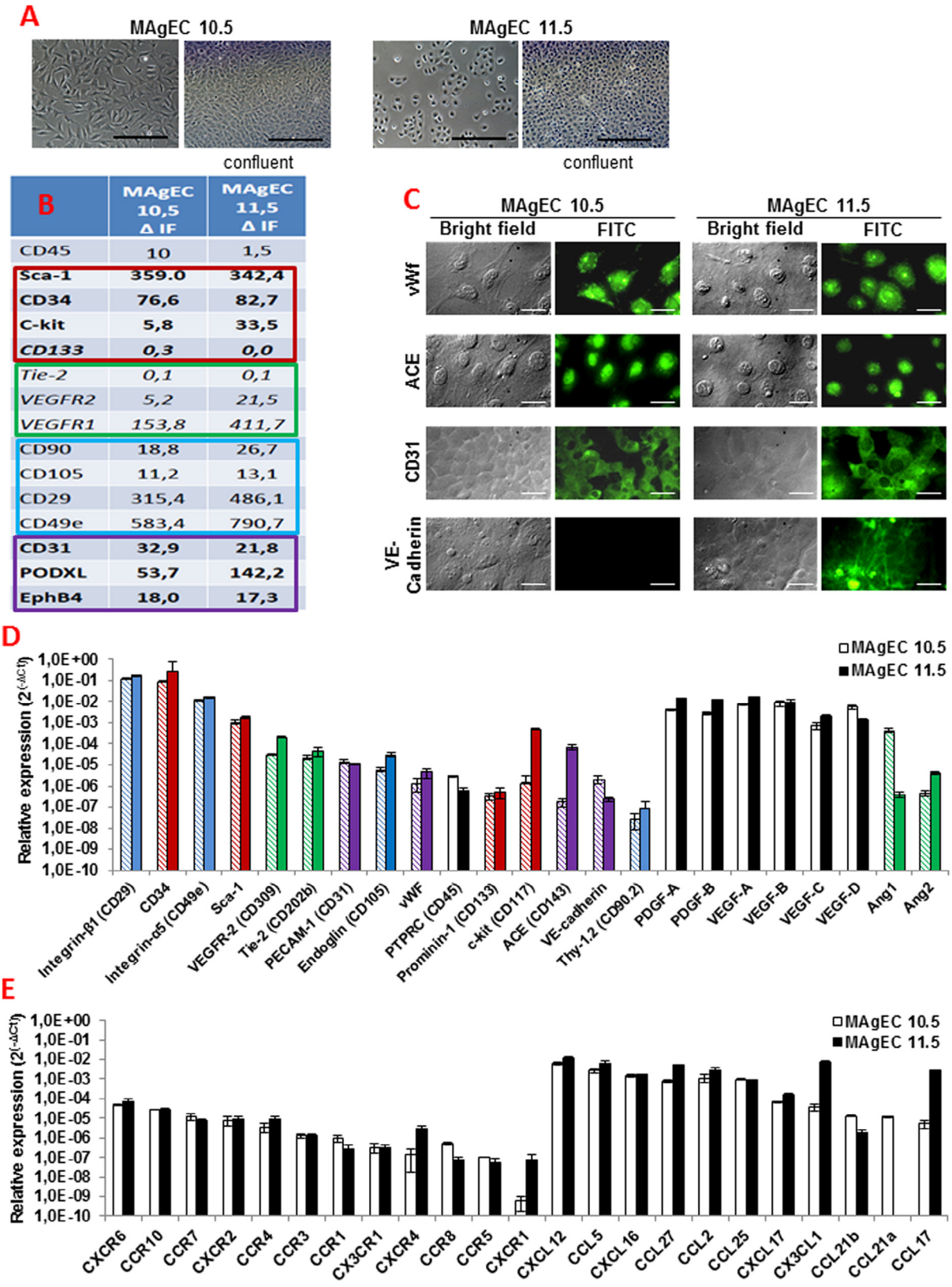

B	MAgEC 10,5 Δ IF	MAgEC 11,5 Δ IF
CD45	10	1,5
Sca-1	359.0	342,4
CD34	76,6	82,7
C-kit	5,8	33,5
CD133	*0,3*	*0,0*
Tie-2	*0,1*	*0,1*
VEGFR2	*5,2*	*21,5*
VEGFR1	*153,8*	*411,7*
CD90	18,8	26,7
CD105	11,2	13,1
CD29	315,4	486,1
CD49e	583,4	790,7
CD31	32,9	21,8
PODXL	53,7	142,2
EphB4	18,0	17,3

Fig. 1. MAgEC characterization of endothelial precursor phenotype. (A) Murine AGM-derived progenitor endothelial cells, MAgEC 10.5 and MAgEC 11.5, cultured as monolayers. Scale bars = 100 μm. (B) MAgEC lines 10.5 and 11.5 cell surface receptor expression analyzed by flow cytometry. Table results represent the difference of the mean cell fluorescence intensity upon binding of the selected antibodies as described in the Materials and methods vs their isotype controls. Results are expressed in ΔIF. (C) Immunocytochemical staining of MAgECs 10.5 and 11.5 by endothelial cell markers antibodies: anti-vWF, anti-ACE, anti-CD31 and anti-VE-cadherin antibodies (green). Scale bare = 20 μm. (D, E) mRNA gene expression by EPCs, histogram D represents the normalized qPCR mRNA expression for endothelial adhesion molecules, endothelial cytokines and their receptors. Histogram E represents expression of mRNAs for chemokines and chemokine receptors. Results are normalized using the house keeping PPIA gene (peptidylprolyl isomerase A/cyclophilin A) and expressed as $2^{-\Delta Ct}$. Values are mean ± SD (n = 3). (For interpretation of the references to color in this figure legend, the reader is referred to the web version of this article.)

The absence of CD45 excluded a commitment toward the hematopoietic lineage. As stem cell marker was detected at the surface of EPCs, c-kit is poorly expressed on MAgEC 10.5 but is present on MAgEC 11.5. Interestingly, both MAgEC lines also express EPCs/mature endothelial cell markers such as PECAM (CD31), von Willebrand factor (vWF), angiotensin converting enzyme (ACE) and the L-selectin ligand, Podocalyxin-like protein 1 (PODXL), while expression of EphB4 indicates a venous vessel commitment.

These markers are indicative but not exclusively typical for endothelial cells and their precursors. EPC markers like VEGFR2 (KDR) are poorly expressed or not detected like the prominin (CD133) and Tie-2, the receptor for angiopoietins 1 and 2.

Differences in the expression of the endothelial differentiation markers appear between MAgEC10.5 and 11.5 indicating a more advanced differentiation of the MAgEC11.5 toward the endothelial lineage. Indeed, Fig. 1C shows the presence of endothelial intracellular markers: ACE, vWF and PECAM-1 (CD31) in both cell lines, but VE-cadherin (CD144) expression is restricted to MAgEC 11.5 cells which express also higher levels of PODXL protein than MAgEC 10.5 (Fig. 1B).

These data were confirmed at the mRNA expression level measured by qPCR and reported in Fig. 1D. All detected markers for stem (Sca-1, CD34), mesenchymal (CD29, CD49, CD90 and CD105) and endothelial lineage (CD117, CD31, vWF, ACE) had a high mRNA expression. Distinctions appeared in CD309, CD133 and CD202 as their mRNAs are highly expressed while the protein was not detected. The endothelial factors were assessed showing that mRNAs for the main pro-angiogenic and regulatory molecules (VEGF-A, -B, -C and-D, Angiopoietin 1 and 2, PDGF-A and -B) were expressed by both cell lines.

MAgEC10.5 and MAgEC11.5 functional characteristics in chemoattraction and response to hypoxia

Angiogenic process depends on parameters as chemoattraction and hypoxia.

Chemoattraction potential was analyzed through the expression of mRNAs for a set of chemokines and their receptors. Fig. 1E shows the expression of the chemokine receptors involved in the cell invasion as CXCR4 and CCR7 as well as their ligands. CXCL12 is produced by both cells but it is remarkable that, as opposed to CCL21b, CCL21a is detected in MAgEC10.5 only. Moreover, MAgEC 11.5 differ from 10.5 by their higher level of expression of CX3CL1and CCL17 chemokines.

As hypoxia is a feature important in embryonic development, stem cell niches and tumor environment where cancer stem cells and endothelial precursors play crucial interactions, the phenotype of MAgECs was analyzed both in normoxic and hypoxic conditions, with regards to the functional markers of endothelial precursors. Fig. 2A reports the differential expression of the genes in hypoxia vs normoxia. The genes as CD143(ACE) and VEGF-A, which were differentially expressed upon hypoxia (Fig. 2A), confirmed a more advanced differentiation of MAgEC 11.5 toward the endothelial lineage as compared to MAgEC10.5. This was corroborated by Sca-1 expression which increased upon hypoxia, in MAgEC10.5 only. Importantly, hypoxia induced a clear increase in Ang2 in both lines, which was accompanied by a reduced expression of Ang1 upon hypoxic treatment.

Hypoxia had a direct impact on the chemokines and chemokine receptor pattern of expression (Fig. 2B). Mostly modulated are the CCL21, a and b, that are involved in the recruitment of CCR7+ cells, while CCR10 overexpression indicates a response to CCL28. CXCL17 (also called VEGF co-regulated chemokine-1) increase corresponds to VEGF co-regulatory effect in hypoxia. The CX3CR1 expression increase reflects a possible modulatory effect on non-mature MAgEC10.5 and the CXCL12 (SDF1-α)/CXCR4 increase on both lines in hypoxia similarly to the CCL27 (CTACK)/CCR10 suggests a role of these two strong chemoattraction axes for endothelial precursor cell-mediated tissue invasion.

Modulation of protein expression by hypoxia had to be compared to the mRNA modulation. Fig. 2C indicates that MAgEc11.5 only were able to secrete the growth, permeabilizing and chemottractant factor VEGF-A which was induced by hypoxia. These cells also produced and secreted CX3CL1 (Fractalkine), CCL17 (TARC) and CXCL12 (SDF1-α). Hypoxia upregulated CXCL12 and downregulated CX3CL1. Both lines produced CCL27 (CTACK); CCL5 was produced mainly by MAgEC 10.5. Fig. 2D shows the cytofluometric detection of the corresponding chemokine receptors on MAgECs. CX3CR1 upregulation suggests a possible endocrine type of action on MAgEC 11.5 only. CXCR4, present on both lines in normoxia, was downregulated upon hypoxia in MAgEC 10.5. CCR10, clearly present only on MAgEC11.5 in normoxia, disappeared upon hypoxia treatment. CCR5, as opposed to its ligand, is restricted to MAgEC 11.5 excluding an autocrine activation by RANTES (CCL5). CCR4 expression appeared hypoxia-dependent in both lines and is not related to CCL17 expression. CCR7, although present on both lines, was downregulated by hypoxia and secretion of its ligand CCL21 was not detected. Although both cell lines present features of non-hematopoietic mesenchymal like stem cells and endothelial precursor cells, they do not strictly belong to a defined category. The protein expression data confirm distinct maturation steps of the MAgEC lines.

MAgEC10.5 and MAgEC11.5 functional characterization by angiogenic properties

The angiogenic potential of MAgEC10.5 and 11.5 cells was investigated in a Matrigel assay. Fig. 3A shows that MAgEC11.5 generated tube-like structures and networks within 12 h, starting the tube-like organization as early as 4 h. MAgEC10.5 cells did not form such networks. They did not make closed structures or pseudovessels; only cell-to-cell contacts were detected. This is in favor of an immature phenotype of MAgEC10.5 cells and confirms that MAgEC11.5 are more advanced toward the endothelial differentiation as they form pseudo-tubes in conditions where MAgEC 10.5 did not, in the absence of proangiogenic factors (Fig. 3A).

The differential distribution of chemokines/receptors and the enhanced selective hypoxia-dependent induction of expression among the two MAgEC cell lines prompted us to precise their effects on the early precursor-like cells that MAgEC10.5 putatively represent. Fig. 3B demonstrates that both CX3CL1 and CCL21 acted as maturation factors for MAgEC10.5 by inducing them to achieve tube like formation *in vitro*. This suggests that MAgECs could be recruited under the effect of such chemoattractants into angiogenic sites where neovascularization occurs. This was tested in coculturing MAgEC lines with mature endothelial cells and assessing for pseudo tube formation. Fig. 3C reports the efficient cooperation of both MAgEC lines with each other and with the mature MLuMEC lung microvascular cells to produce pseudo vessels indicating that although MAgEC10.5 cells alone are not able to make vessels, both endothelial precursor cell types could participate to the neovascularization as occurs in the developing tumors.

This was confirmed *in vivo* by the demonstration of MAgEC cells' ability to form functional vessels in an artificially-induced angiogenic site. Matrigel plugs are known to serve as angiogenesis inducers. Fig. 3D shows that ultrasound detection of blood flow inside and around the Matrigel plug indicated a faint angiogenic network in the plug (Fig. 3Da), as confirmed by the fluorescence macroscopic detection (Fig. 3Dg). When the MAgEC cells were incorporated in the Matrigel, angiogenesis was clearly increased as can be

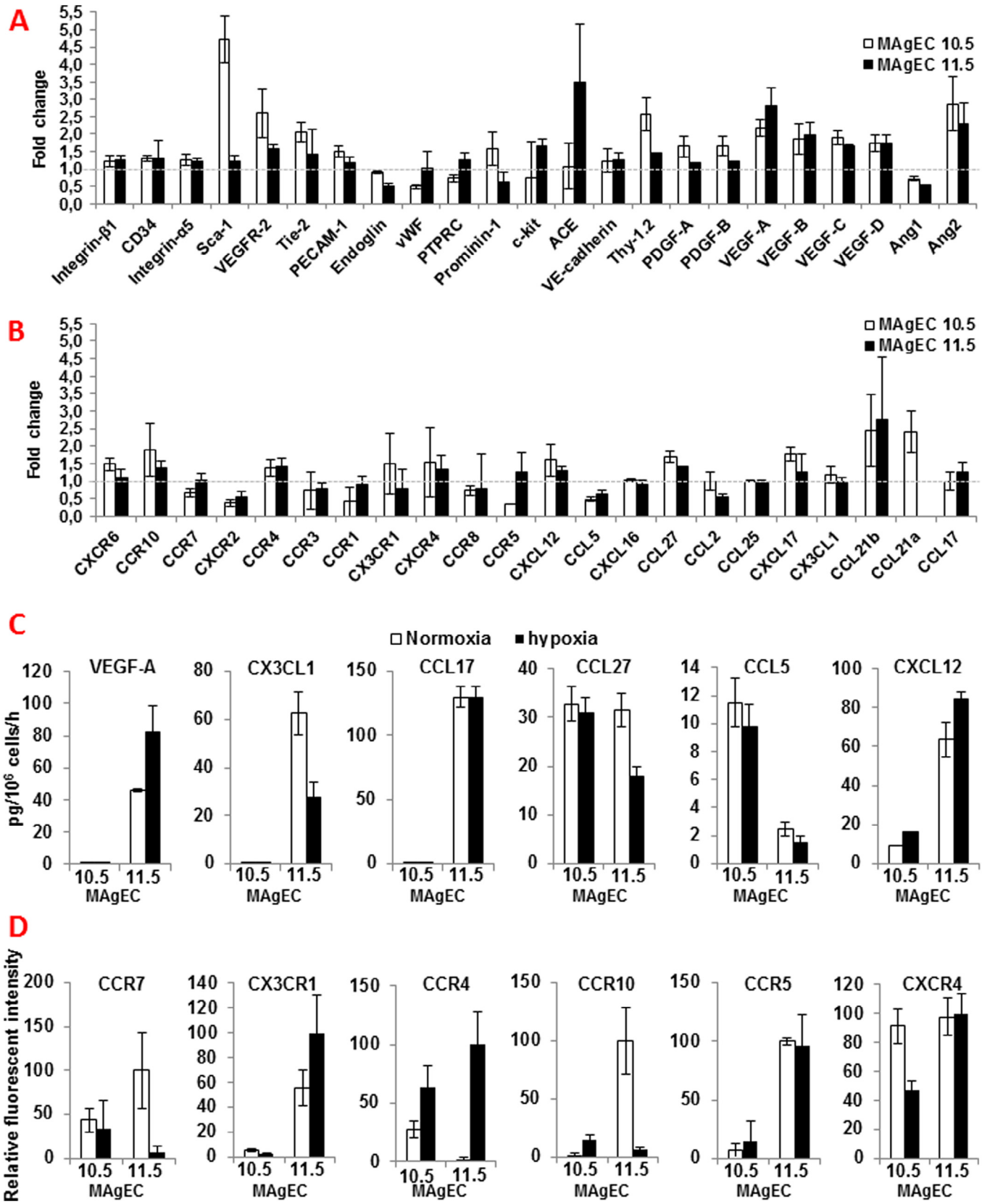

Fig. 2. Modulation of MAgEC gene expression in response to hypoxia. (A) Fold change of endothelial adhesion molecules, differentiation antigens and endothelial function molecules and cytokines and their receptors estimated by qPCR of their mRNA expression in hypoxia vs normoxia. MAgEC 10.5 and 11.5 lines were cultured in 21% O_2 (normoxia) and 1% O_2 (hypoxia). Values are mean ± SD (n = 3). (B) Differential expression of the mRNA estimated by qPCR for various chemokines and chemokine receptors. All results expressed as fold change as in (A). Values are mean ± SD (n = 3). (C) CCR7, CCR 4, CCR 10, 5 CCR, CX3CR1, and CXCR4 chemokine cell surface receptors expression assessed by flow cytometry on MAgEC 10.5 and 11.5 cells cultured for 24 hours under normoxia (21% O_2) and hypoxia (1% O_2). Values are mean ± SD (n = 3). (D) VEGF-A, CX3CL1, CCL17, CCL27, CCL5, and CXCL12 production by MAgEC 10.5 and 11.5 cells cultured for 24 hours in normoxia (21% O_2) and hypoxia (1% O_2). Production was measured by ELISA. Results are reported to 10^6 cells and per hour (h). Values are mean ± SD (n = 3).

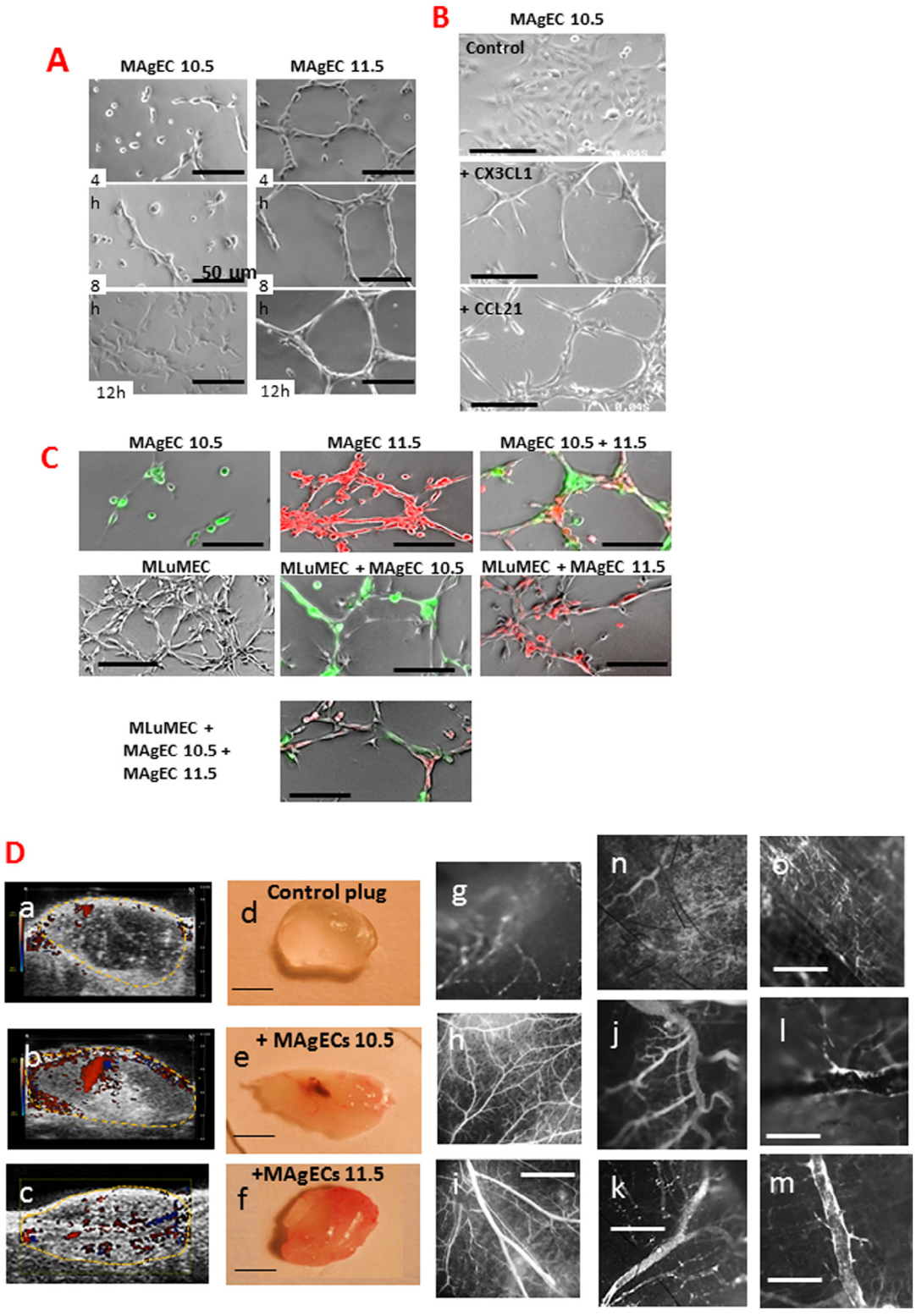

Fig. 3. MAgEC line activity in the angiogenesis process. (A) Representative pictures of tube-like structure formation by Matrigel-plated MAgEC 10.5 and 11.5 cells, incubated for up to 12 h. Scale bars represent 50 µm. (B) MAgEC 10.5 angiogenic response to stimulation by chemokines CX3CL1 and CCL21 in Matrigel assay after 24 h of incubation with chemokines. Scale bars represent 50 µm. (C) Cooperation between MAgEC 10.5, 11.5 and MLuMEC,FVB cell lines in the pseudo tube network formation on Matrigel. The MAgEC 10.5 (green) and MAgEC 11.5 (red) were DiO and DiI labeled, respectively, while MLuMEC remained unlabeled. Pictures represent the networks formed after 24 h of incubation. Scale bars represent 50 µm. (D) Vessel formation *in vivo* and blood flow establishment in functional vessels by MAgEC 10.5 and MAgEC 11.5 in Matrigel plugs evidenced by ultrasonography imaging (echography) combined with Doppler mode (a, b, c). The red and blue colors allow flow direction discrimination: inward and outward flow from the transducer respectively. Representative pictures of control plug (d), or plug mixed with MAgEC 10.5 (e) or 11.5 (f), *in vivo*, one week after grafting in mice. d, e, f: Macroscopic pictures of the corresponding plugs isolated from the mice. Scale bars represent 0.5 cm. Angiogenesis in the control Matrigel plug (g) compared to MAgEC 10.5 cells (h) and MAgEC 11.5 (i) mixed Matrigel plugs and after TRITC-dextran injection and detection by fluorescence macroscopy (n) and (o) are control skin vessels from (h) and (i); bars represent 100 µm. λ_{ex} 543/22 nm, beam splitter 562 nm, λ_{em} LP561 nm were used for TRITC observation as in (j) and (k); bars represent 40 µm. Cell level detection in the FITC channel: λ_{ex} 482/35 nm, beam splitter 506 nm, λ_{em} 536/40 nm for MAgEC10.5 mixed plugs (l) and MAgEC11.5 (m); bar represents 20 µm. (For interpretation of the references to color in this figure legend, the reader is referred to the web version of this article.)

observed from isolated plugs containing MAgEC10.5 (Fig. 3De) and MAgEC11.5 (Fig. 3Df) compared to control plug (Fig. 3Dd), 10 days after implantation, and the formed vessels were functional since an efficient blood flow was established by both MAgEC10.5 (Fig. 3Db) and MAgEC11.5 (Fig. 3Dc) inside the plug compared to the control plug (Fig. 3Da). Structure and function of vessels were assessed by fluorescence macroscopy imaging after i.v. injection of high molecular weight TRITC-labeled dextran. Fig. 3D presents the vessel network formed in plugs containing MAgEC10.5 (Fig. 3Dh) and MAgEC11.5 cells (Fig. 3Di). The detailed structures formed in plugs containing MAgEC10.5 and MAgEC11.5 are presented in Fig. 3Dj and 3Dk, showing the fluorescence of vessels containing TRITC–Dextran and the observation by FITC channel displayed the vessel walls in the case of MAgEC10.5 (Fig. 4Dl) and MAgEC11.5 (Fig. 3Dm). The structure of the vasculature in normal skin tissue is shown in Fig. 3Dn and Do for mice that have been implanted with plugs containing MAgEC10.5 and MagEC11.5 respectively. A general view of the plug vascularization is given in Supplementary Fig. S1a together with a detailed structure of vessels which contain the FITC–dextran (Supplementary Fig. S1b, c).

MAgEC10.5 and MAgEC11.5 cells are actively recruited by spheroid tumor models in vitro *and proangiogenic sites* in vivo

Future use of EPCs for therapeutic purposes, on the basis of models of differentiation provided by MAgEC10.5 and/or MAgEC11.5, requires the determination of their response to tumor mediated chemoattraction. An *in vitro* assay was designed to image the interaction and possible recruitment of MAgEC cells by a growing tumor in a spheroid model. To mimic cell–cell cooperation in a tumor site, the experiment reported in Fig. 4A was set in a melanoma tumor model. The B16F10 melanoma model was used as it represents a hypoxic tumor model which we studied for its answer to blood vessel normalization by our second strategy using allosteric effector of hemoglobin [40] and to the expression of hypoxia-conditioned soluble VEGF receptor 2, *in vivo* [26]. Fig. 4A shows spheroids resulting from mixing fluorescent B16F10 with nonlabeled mature MLuMEC as mature endothelial cells. Green fluorescent MAgEC11.5 cells were then seeded into the surrounding Matrigel and detected by their green fluorescence for tracking. They approached the spheroids. Indeed, spheroids were rapidly surrounded by MAgEC11.5 (Fig. 4A, white arrows) which, after 24 hours, entered the spheroids (Fig. 4B) as shown by confocal microscopy, allowing tracking spheroid invasion by MAgEC11.5 cells. Moreover, cells which invaded the spheroid formed vessel-like structures within 72 hours, in and around the tumor-like structure (Fig. 4C, white arrows). MAgEC11.5 invasion of the spheroids was also quantified by cell counting in confocal microscopy (Fig. 4D) and image analysis to track the MAgEC cells inside the spheroids. These cells were not attracted by invasion of tumor spheroids is an active process since these cells were not attracted toward fixed spheroids (Fig. 4E). Mature endothelial cells, MLuMEC, invaded efficiently the spheroids and the MAgEC11.5 and MAgEC10.5 cells did comparably in normoxia (21% O_2). To mimic the tumor microenvironment, the cell model was incubated in hypoxia (1% O_2, after preconditioning the cells as routinely done for 24 hours in hypoxia), in which conditions we routinely established that the hypoxia inducible factor (HIF-1α) protein expression is stable for 48 hours as measured (Supplementary Fig. S2) and HIF-dependent genes activated as previously published [40]. Hypoxic conditions influenced the profile of recruitment for mature endothelial cells (fold increase 1.8) and MAgEC11.5 (fold increase 1.94), especially pointing to the MAgEC10.5 precursor cells which were better recruited than in normoxia (fold increase 4.64) compared to the more differentiated endothelial precursors (MAgEC11.5) and especially to the mature endothelial cells (Fig. 4E, inset).

MAgEC10.5 and MAgEC11.5 incorporate into proangiogenic sites in vivo *and mediate the targeted expression of a therapeutic gene*

MAgEC's ability to be recruited by tumors was validated *in vivo* using an assay that allows cell tracking. GFP-expressing MAgEC10.5 and MAgEC11.5 cells (Fig. 5A) were intravenously injected to mice implanted with Matrigel plugs containing VEGF and FGF to induce angiogenesis. Flow cytometry detection and quantification of labeled cells among various organs and in the Matrigel plug allowed quantification of MAgEC10.5 and MAgEC11.5 present into proangiogenic sites. Flow cytometry data (Fig. 5B) show a preferential localization of the MAgEC10.5 and MAgEC11.5 into the plugs as quantified 10 days after injection, a sufficient time to allow homing and recirculation. Moreover the selectivity of endothelial precursor cells for proangiogenic sites represented by the Matrigel plug is shown in comparison with mature endothelial cells (inset) after 7 days. To identify the cells that are present at the vessel formation level and assess for the participation of MAgEC 10.5 and/or MAgEC 11.5 cells, the histochemical labeling for CD31 was examined and compared to the detection of the DiD-labeled MAgEC10.5 and MAgEC11.5 cells. Fig. 5Ca shows that the DiD labeled MAgEC10.5 cells present a colocalization with CD31+ cells at the delineation of the vessels, the same can be observed with MAgEC11.5 cells in Fig. 5Cb where the DiD labeled cells co-localize with CD31 on vessel-like structures and in Fig. 5Cc the DiD labeled MAgEC11.5 cells enter the vessel structure. Moreover expression of VEGFR2 was detected on MAgECs in the plugs and shown co-localization with the fluorescent DiD label of MAgEC11.5 in Fig. 5Cd. A more general view of the plugs containing MAgEC10.5 cells (Fig. 5Ce) and MAgEC11.5 cells (Fig. 5Cf) indicated CD31+ alignment in vessel-like structures. The data were extended to tumor bearing animals. The tumor progression is linked to angiogenesis; consequently, MAgECs were tested for their potential recruitment into the tumor site and incorporation into the tumor vasculature.

MRI detection of AMNP-labeled cells reported in Fig. 5D shows a hypodense concentration of the label 24 hours after injection of labeled MAgEC11.5 cells, detected at the tumor site in aligned structures evoking vessels (Fig. 5D, arrows). MRI signal was detected in other organs as spleen (not shown). Consequently, in order to rule out a possible effect of paramagnetic marker, fluorescent lipid-labeled MAgEC11.5 cells were injected to tumor bearing mice and tracked by flow cytometry. The cells were quantified on the basis of their fluorescence by flow cytometry (Fig. 5E) in the tumor (0.018% ± SD positive) and other organs: spleen (0.008% ± SD positive), lungs (0.005% ± SD positive), bone marrow (0.02% ± SD positive) and lymph nodes (almost no fluorescent cell detected), indicating that the MRI signal indeed corresponds to the injected MAgEC cells.

In these experiments B16F10, 7 day tumor-bearing mice, were intravenously injected with DiI-labeled-MAgEC11.5, -MAgEC10.5 cells or mature microvascular endothelial cells from lung (MLuMEC), brain (MBrMEC), bone marrow (MBMMEC) or spleen (MSplMEC), then cell homing, recirculation and settlement were allowed for 9 days. The numbers of DiI-labeled MAgEC cells were assessed in organs and tumor, after tissue dilaceration and detection by flow cytometry. Fig. 5F reports the number of MAgEC11.5 cells localized in the various organs per mass unit of tissue. When reported to the whole organs, numbers indicate that MAgEC11.5 cells were found preferentially inside the tumor site (12.5–20% ± SD of the injected cells) and the bone marrow (3–4% ± SD of the injected cells). The numbers of MAgEC11.5 found among the other organs ranged from 0.01% ± SD in thymus, 0.2% + SD in lymph nodes, up to 0.4% ± SD circulating in the blood. Supplementary Fig. S3 shows that MAgEC10.5 displayed similarly a preferential localization in the tumor and the bone marrow. Other endothelial cell lines were not preferentially recruited inside the tumor. Further similar experiments were undertaken to assess the effectiveness of endothelial precursor cells

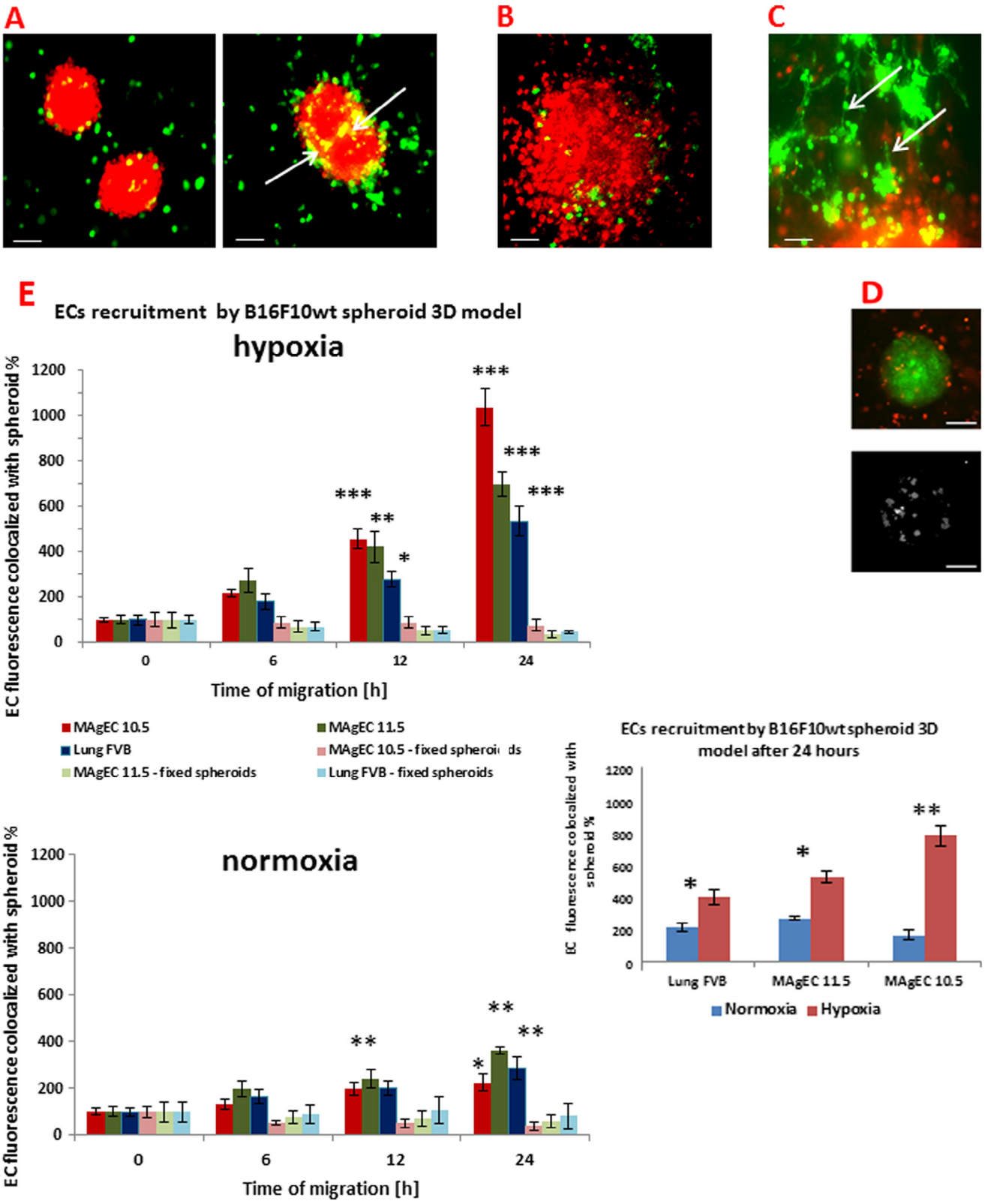

Fig. 4. 3D models of MAgEC10.5 and MAgEC11.5 cells' invasive ability toward B16F10 melanoma spheroids. (A) B16F10 melanoma (red) mixed to MLuMEC (from 100 to 1) spheroids into a collagen/methylcellulose matrix mixed with MAgEC 11.5 cells (green). Left: 6 h of incubation. Right: 24 h of incubation. Scale bar = 250 μm. (B) Confocal fluorescence microscopy of melanoma spheroid, incubated 24 h with MAgEC 11.5 cells. Scale bar = 50 μm. (C) 3D tube-like organization into the matrix of the fluorescent green labeled MAgEC 11.5 cells near a B16F10 melanoma spheroid upon incubation in hypoxia (1% O_2). Scale bar = 20 μm. (D) Quantification of the spheroid-invading MAgEC 11.5 cells by fluorescence microscopy image analysis. Scale bar = 100 μm. (E) MAgEC10.5, MAgEC 11.5 endothelial precursors cells and MLuMEC,FVB mature endothelial cells recruited by melanoma spheroids in normoxia (18.75% of O_2) compared to hypoxia (1% of O_2). Bars represent mean ± SEM. Values significantly different from T = 0 h were marked with: * $p < 0.05$; ** $p < 0.01$; *** $p < 0.001$. Inset compares relative recruitment of endothelial cells in hypoxia vs normoxia for MLuMEC,FVB (R = 1.87), MAgEC 11.5 (R = 1.94) and MAgEC 10.5 (R = 4.64). Bars represent mean ± SEM. Values significantly different between normoxia and hypoxia were marked with: * $p < 0.05$; ** $p < 0.01$. Graphs report the analysis and quantification obtained with "RG2B colocalization" ImageJ software plug-in. Controls were "fixed" spheroids as opposed to "alive" spheroids (N > 10). (For interpretation of the references to color in this figure legend, the reader is referred to the web version of this article.)

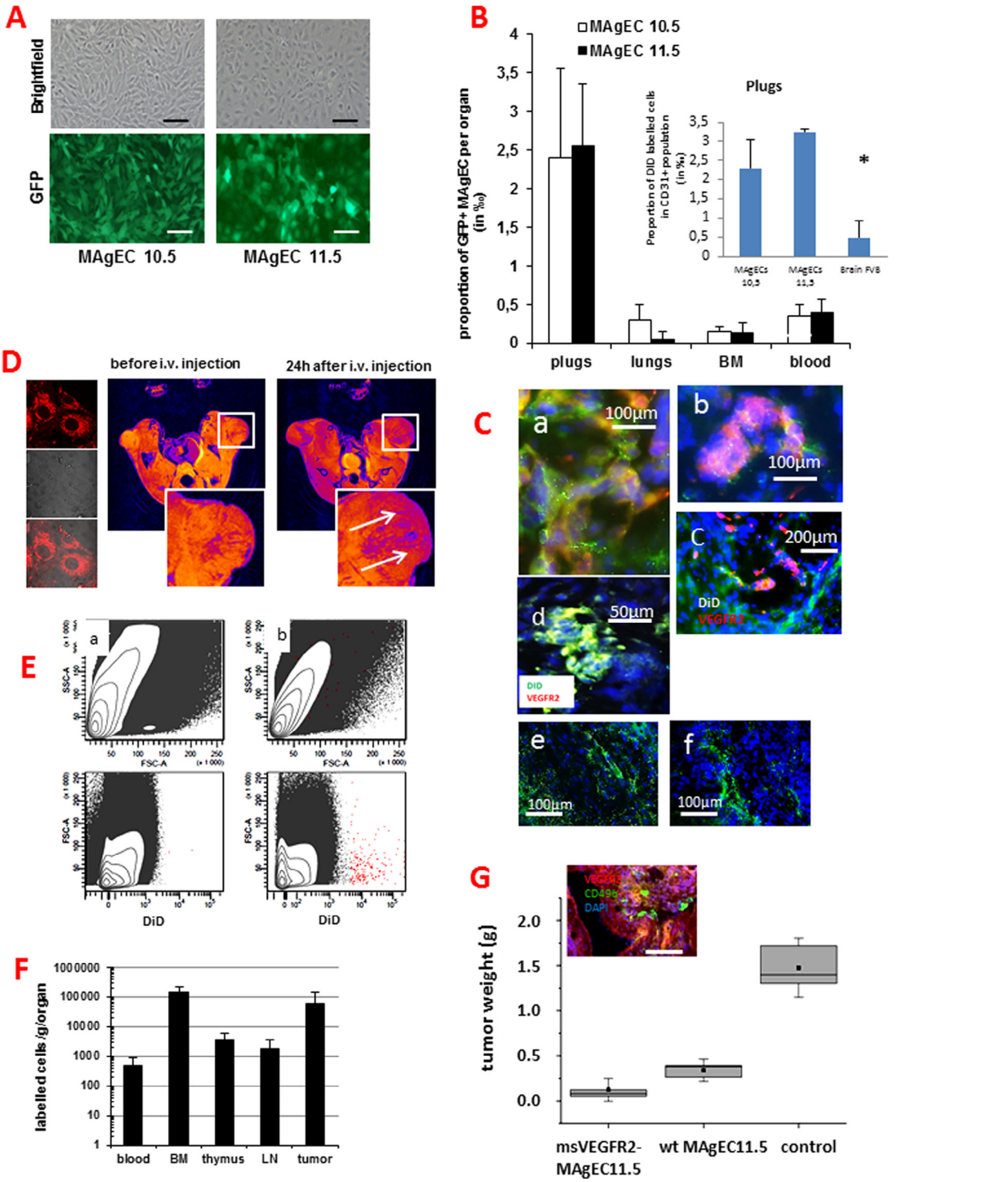

Fig. 5. *In vivo* homing abilities of MAgEC cells into tumor bearing mice. (A) GFP expressing stable cell lines of MAgECs10.5 and 11.5, in bright field, fluorescence. Bars = 20 µm. (B) Flow cytometry data of the percentage of MAgECs-GFP+, 10.5 and 11.5, found in distinct organs of mice bearing Matrigel-plugs (10 days) after dissociation of plugs, lungs, bone marrow (BM) and in blood. Results are ‰ of total cells from each tissue. Values are mean of 3 examined mice ± SD (n = 3). Inset: Preferential homing of MAgEC10.5 and MAgEC11.5 cells vs mature endothelial cells from brain, 7 days after injection. Values are mean of 3 examined mice ± SD (n = 3). (C) Histochemical detection of MAgEC10.5 and MAgEC11.5 cells invading plugs (7 days post i.v. injection). (a) MAgEC10.5 DiD-labeled cells found in plugs colocalizing with CD31; (b, c) MAgEC11.5 DiD-labeled invading vessel-like structures and (d) displaying VEGFR2 expression. CD31+ cells distribution in plugs containing MAgEC10.5 (e) and MAgEC11.5 cells (f). (D) MAgECs11.5 cells loaded with rhodamine-labeled superparamagnetic beads. (a) Representative picture in fluorescence microscopy. Top: fluorescence, middle: bright field, low: merge. (E) Magnetic resonance imaging of melanoma bearing mice: before intravenous injection of rhodamine-labeled superparamagnetic beads loaded into MAgEC11.5 cells (b) and 24 h post injection (c). (E) Flow cytometry quantification of tumor-homing MAgECs. Dot plots evidence the labeled MAgEC11.5 cells found in the 16-day melanoma tumor after *i.v.* injection/homing of 10^6 DiD-labeled MAgEC11.5 cells and recirculation for 7 days (b). Controls are fixed DiD-labeled MAgEC11.5 cells (a). (F) Flow cytometric quantification of labeled MAgEC11.5 cells among various organs of 16-day melanoma tumor bearing mice, 7 days after intravenous injection of MAgEC11.5 cells. Values are mean ± SD (n = 3). (G) Weight of 16-day B16 melanoma tumors, 7 days after i.v. injection of 10^6 MAgEC11.5 cells (wild type and transfected by the msVEGFR2 hypoxia-dependent expressing vector – msVEGFR2-HRE). Controls were obtained by injection of fixed MAgEC11.5 cells. Reported values are mean ± SD from 5 examined mice. Inset: histochemical detection of CD49b+ cells (green) invading tumor mass (VEGFR2+) after injection of MAgEC11.5 cells (Bar = 50 µm). (For interpretation of the references to color in this figure legend, the reader is referred to the web version of this article.)

to carry a therapeutic gene as msVEGFR2-HRE which was designed and validated as hypoxia-conditioned for the synthesis of ms-VEGFR2 and reversible upon hypoxia compensation and vessel normalization [26]. MAgEC11.5 clone 131 (Supplementary Fig. S4) was chosen for its high differential expression of msVEGFR2 in hypoxia vs normoxia (R = 25). smVEGFR2-HRE-MAgEC11.5 cells and -MAgEC11.5 cells were DiI labeled, injected in B16F10 bearing mice 7 days after tumor implantation and their effect was measured on the tumor development, 9 days after injection. They displayed a similar homing pattern and cell recovery confirmed above data (Supplementary Fig. S5). A better reduction of the tumor size was observed in mice treated by msVEGFR2-HRE-MAgEC11.5 cells as compared to the effect observed in mice treated by MAgEC cells (Supplementary Fig. S5, inset). Fig. 5G confirms these data and also points to the effect of the non-transfected endothelial precursor cells in reducing the tumor growth compared to the injection of mature endothelial cells (Supplementary Fig. S6). As before, this effect is enhanced with msVEGFR2-HRE-MAgEC11.5 cells, expressing the therapeutic msVEGFR2 hypoxia-dependent gene (Supplementary Figs. S5 and S6 and Fig. 5G). MAgEC cell injection and their localization in the tumor vasculature (Supplementary Fig. S6B) might impact the immune cell recruitment. As previously shown with angiogenesis treatment, CD49b+ NK cells are detected inside the tumor mass [41], as shown by the preliminary data reported in Fig. 5G (inset), which were not observed in control tumors. When B16F10 spheroids were used as tumor models and the selected clones of MAgEC11.5 and 10.5 transfected by msVEGFR2-HRE-vector (Supplementary Fig. S4) were used to treat the tumor bearing mice, the above data were confirmed (Supplementary Fig. S6) and corroborate our previous findings [26] on therapeutic hypoxia-conditioned expression of the msVEGFR2 as a VEGF regulator.

Discussion

This work proves the feasibility of using properly defined endothelial precursor cells as a tool for tumor targeting because of their ability to be naturally and specifically recruited to sites where active angiogenesis takes place, namely in solid tumors [42], and the possibility to make them carry therapeutic drugs or genes [25,36].

Our purpose, in selecting a good cellular candidate, was to obtain the early precursor committed to endothelial phenotype during embryonic development which will be the appropriate cell to incorporate a proangiogenic site. This was supposed to allow the determination of the maturation step at which endothelial precursor cell represents the best cells to control vasculogenesis.

The first cells restricted to the endothelial lineage appear in aorta–gonad–mesonephros (AGM) during mouse embryogenesis [28]. In the mouse embryo they diverge from hemangioblasts at 10.5 and 11.5 days post conception (dpc) [27]. From AGM, two cell lines were established, called MAgEC 10.5 and MAgEC 11.5, to allow their use as cell models because of the phenotypic stability reached upon immortalization [43,44] as compared to isolated primary EPCs.

Characterization indicated that such early precursors could be classified as EPCs, although they did not share all described EPC features. They were distinctly committed toward the endothelial phenotype. Indeed, the two lines displayed progenitor endothelial characteristics reflecting distinct maturation stages in terms of phenotype and angiogenic properties. Moreover, they cooperated with mature endothelial cells in the formation of angiogenic network which corresponds to a hallmark of recruited EPCs.

Historically, endothelial precursor cells were initially identified and isolated on the basis of vascular endothelial growth factor receptor-2 (VEGFR2) and CD34 co-expression [1]. Since this brief cell description, which is still debated and, in the light of the ongoing knowledge on stem cells combined to the emergence of specific surface markers, numerous distinct populations of stem and progenitor cell populations were identified at various steps of differentiation, making cell populations overlap along the differentiation continuum. However, "specific" markers are chosen to facilitate the isolation and purification of these cells but the increasing number of markers makes it more complex the definition of "true" EPCs among EPC-like cells. Generally admitted, the term "EPC" may encompass a group of cells existing in a variety of stages ranging from primitive hemangioblasts to fully differentiated ECs.

EPC cells should express several markers (Fig. 6) including VEGF receptor-2 (VEGFR2, KDR, Flk-1), VE-cadherin, CD34, platelet endothelial cell adhesion molecule (PECAM; CD31) and von Willebrand factor (VWF). They should also be able to bind acetylated low-density lipoprotein (AcLDL) and lectins such as *bandeiraea simplicifolia* agglutinin-1 (BSA-1) and *ulex europaeus* agglutinin-1 (UEA-1) which are usually considered as endothelial-specific markers [2,45]. Thus, characterization of EPCs remains complex. Despite controversial data on the EPC identity and classification [3–6], circulating endothelial precursors' involvement in physiological and pathological processes was shown [7–12].

Considering the characteristics of the MAgEC lines and according to the data obtained by *in vitro* and *in vivo* investigations which show their ability to home specifically into neoangiogenic sites, they should provide an effective cell model of EPC *in vivo*. Moreover, endothelial precursors, at this step of differentiation, represent good candidates for cell transplantation due to their low expression of histocompatibility antigens [46] and thus for the delivery of therapeutic genes [2,26,47]. This is corroborated by their sensitivity to B16F10 melanoma-secreted signals as observed *in vitro* in a model of micro-tumor inducing an active migration of these cells toward the tumor site. This was confirmed by the ability of MAgEC cells to home, *in vivo*, into a B16F10 tumor site and to be a good cell carrier for tumor cell-based gene therapy.

Indeed, EPCs appear to be a tool of choice for angiogenesis targeting in view of tumor therapy (Fig. 6). Due to their quiescent character in normal conditions circulating EPCs, upon incorporating into the endothelium, should allow long-term expression of therapeutic genes, making them the mean for the so-called "Trojan Horse" approaches [48]. Their use to reach the tumor site should prevent the lack of specificity observed with classical therapies and consequently should reduce potential side effects.

The numerous approaches to target angiogenesis were designed first to destroy this pathologic process, while it is now aimed to normalize vessels in order to make them efficient for treatment delivery [49]. Normalization is by now recognized as an alternative to the antiangiogenesis strategies and long term normalization is the key to adjuvant anticancer strategies [50].

We have designed five complementary approaches toward tumor vessel normalization for treatments based on hypoxia compensation [40], microRNA regulation [47,51], hypoxia-regulated gene therapy [26], plasma-mediated blood flow increase [52] and normal endothelial cells recruitment to help recover normal vessel functionality. Such therapies present advantages over classical ones by improving the ratio benefits/side effects and give the possibility to be introduced into conventional protocols involving chemo and/or radiotherapy [49] and act synergistically [40].

As presented in this manuscript, by providing a model cell line for EPCs, our work helps to design improved cell therapies and provides tools for new normalization-based strategies. This model allows bringing together the tumor natural targeting and therapeutic gene of which expression is microenvironment conditioned. This combined strategy is able to reduce the tumor growth by alleviating tumor hypoxia thus deeply changing the microenvironment of the tumor cells [38] to such an extent that the immune response is considerably boosted. Our data on NK cell recruitment indicate that treating tumor angiogenesis by endothelial precursor cell targeting participates to this effect. It represents a good model to shape

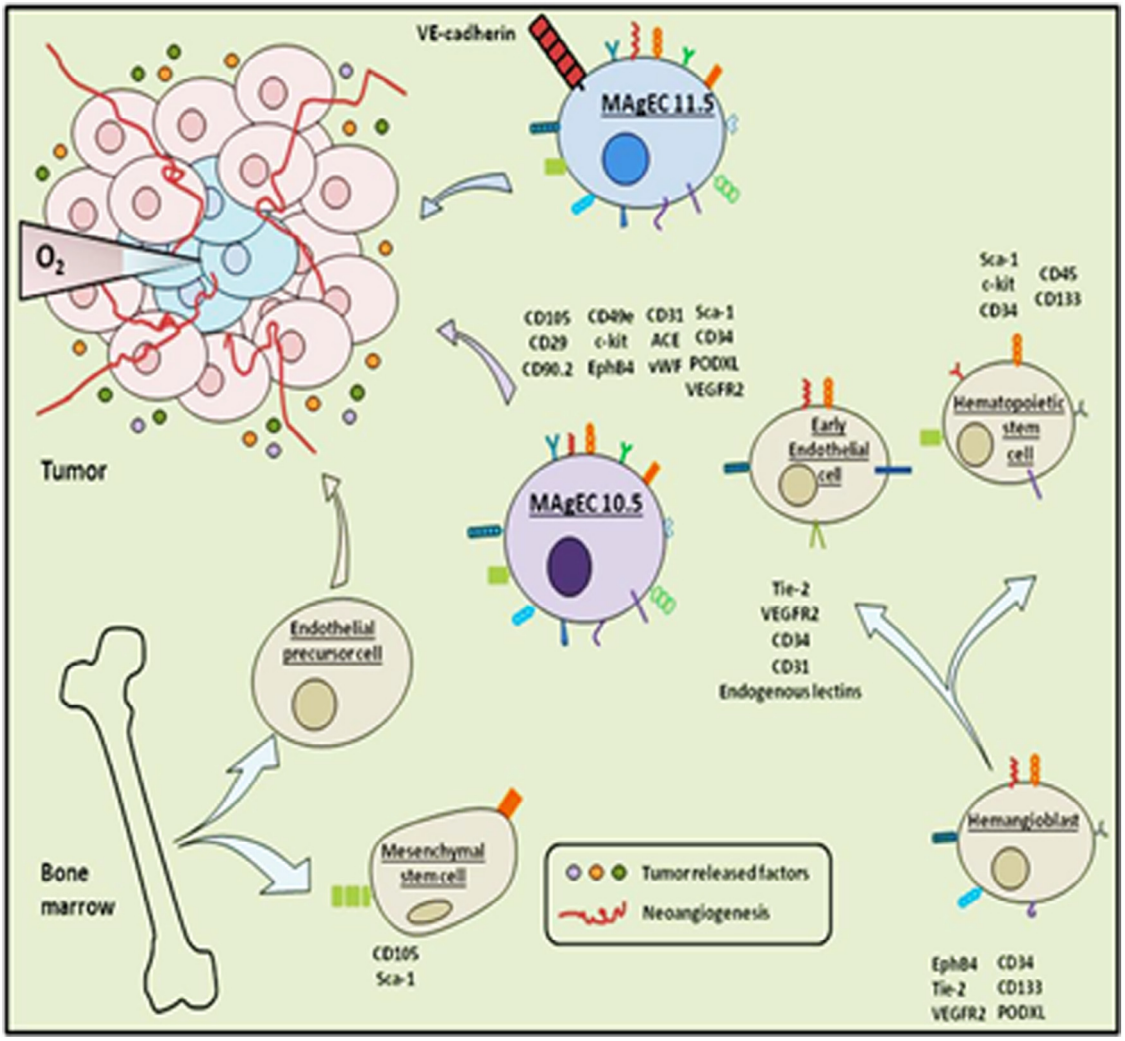

Fig. 6. MAgEC characterization scheme by specific marker expression. Tumor targeting cells including endothelial precursor cells (EPCs), mesenchymal stem cells (MSCs), early endothelial cells, hematopoietic stem cells and hemangioblast to identify the markers shared by MAgEC cells and point out their possible use as tumor targeting cells as compared to EPCs.

the induced pluripotent stem cell iPS differentiation into endothelial precursor cells [36,53] or take advantage of the endothelial to mesenchymal transition [54] to obtain the cell phenotype enabling an efficient targeting.

Authors' contributions

Conceived and supervised the study: CK, JD. Conceived and designed experiments: GC, CK, JD. Performed the experiments: GC, KSz, WN, K Szc, DS, KW, AFC, AG, AM, BEHR, KK, FF, NLF. Analyzed the data: GC, KSz, WN, JCB, AJ, CK, JD. Contributed reagents/materials/analysis tools: GC, KSz, WN, KSzc, DS, KW, AG, AM, BEHR, KK, NLF, JD, JCB, MN, CG, SP. Drew Fig. 6: MN. Wrote the manuscript: GC, CK.

Acknowledgements

This paper is dedicated to the memory of the late Pierre Smirnov (PhD).

We thank Dr Pierre Smirnov for the MRI experiments, David Gosset for the help in flow cytometry technique and for cell sorting, Frederic Szeremeta for MRI data analysis, Dr Florence Gazeau (MSC laboratory, CNRS/University Paris Diderot, Paris France) for kindly providing us with the Anionic Magnetic NanoParticles (AMNP). We wish to thank Michèle Mitterrand (CBM-CNRS Orléans) for preliminary series of cell homing and tumor targeting experiments.

Guillaume Collet was a doctoral fellow sponsored by the French Ministry of Research; fellowship No. 32852-2008, the Malopolska Marshal Office and the LNCC (National League Against Cancer).

This work was partly supported by the French-Polish Grant INCa/CNRS/MNiSW (347/N-INCA/2008) for cooperation and ANR "triple sens project", the LNCC, the Institut National de la Santé et de la Recherche Médicale (INSERM), the FEDER MiRPeau 5788/39114; the Harmonia Project No. 2012/06/ M/NZ1/00008 supported by the National Science Center and "La Ligue Régionale contre le Cancer" and the EU Framework Programs POIG 02.01.00-12-064/08 and 02.02.00-00-014/08. Faculty of Biochemistry, Biophysics and Biotechnology of Jagielloian University is a partner of the Leading National Research Center (KNOW) supported by the Ministry of Science and Higher Education. Research has been conducted in the scope of the MiR-TANGo International Associated Laboratory (LIA).

Conflict of interest

Authors declare no conflict of interest.

Appendix: Supplementary material

Supplementary data to this article can be found online at doi:10.1016/j.canlet.2015.11.008.

References

[1] T. Asahara, T. Murohara, A. Sullivan, M. Silver, R. van der Zee, T. Li, et al., Isolation of putative progenitor endothelial cells for angiogenesis, Science 275 (1997) 964–967.
[2] C. Urbich, S. Dimmeler, Endothelial progenitor cells: characterization and role in vascular biology, Circ. Res. 95 (2004) 343–353.
[3] D.A. Ingram, N.M. Caplice, M.C. Yoder, Unresolved questions, changing definitions, and novel paradigms for defining endothelial progenitor cells, Blood 106 (2005) 1525–1531.
[4] G. Krenning, M.J. van Luyn, M.C. Harmsen, Endothelial progenitor cell-based neovascularization: implications for therapy, Trends Mol. Med. 15 (2009) 180–189.
[5] E. Pasquier, S. Dias, Endothelial progenitor cells: hope beyond controversy, Curr. Cancer Drug Targets 10 (2010) 914–921.
[6] M.C. Yoder, D.A. Ingram, Endothelial progenitor cell: ongoing controversy for defining these cells and their role in neoangiogenesis in the murine system, Curr. Opin. Hematol. 16 (2009) 269–273.
[7] D. Gao, D.J. Nolan, A.S. Mellick, K. Bambino, K. McDonnell, V. Mittal, Endothelial progenitor cells control the angiogenic switch in mouse lung metastasis, Science 319 (2008) 195–198.
[8] J.M. Hill, G. Zalos, J.P. Halcox, W.H. Schenke, M.A. Waclawiw, A.A. Quyyumi, et al., Circulating endothelial progenitor cells, vascular function, and cardiovascular risk, N. Engl. J. Med. 348 (2003) 593–600.
[9] A.S. Mellick, P.N. Plummer, D.J. Nolan, D. Gao, K. Bambino, M. Hahn, et al., Using the transcription factor inhibitor of DNA binding 1 to selectively target endothelial progenitor cells offers novel strategies to inhibit tumor angiogenesis and growth, Cancer Res. 70 (2010) 7273–7282.
[10] D.J. Nolan, A. Ciarrocchi, A.S. Mellick, J.S. Jaggi, K. Bambino, S. Gupta, et al., Bone marrow-derived endothelial progenitor cells are a major determinant of nascent tumor neovascularization, Genes Dev. 21 (2007) 1546–1558.
[11] B.A. Peters, L.A. Diaz, K. Polyak, L. Meszler, K. Romans, E.C. Guinan, et al., Contribution of bone marrow-derived endothelial cells to human tumor vasculature, Nat. Med. 11 (2005) 261–262.
[12] J. Sasajima, Y. Mizukami, Y. Sugiyama, K. Nakamura, T. Kawamoto, K. Koizumi, et al., Transplanting normal vascular proangiogenic cells to tumor-bearing mice triggers vascular remodeling and reduces hypoxia in tumors, Cancer Res. 70 (2010) 6283–6292.
[13] A.J. Horrevoets, Angiogenic monocytes: another colorful blow to endothelial progenitors, Am. J. Pathol. 174 (2009) 1594–1596.
[14] J. Rehman, J. Li, C.M. Orschell, K.L. March, Peripheral blood "endothelial progenitor cells" are derived from monocyte/macrophages and secrete angiogenic growth factors, Circulation 107 (2003) 1164–1169.
[15] E. Rohde, C. Malischnik, D. Thaler, T. Maierhofer, W. Linkesch, G. Lanzer, et al., Blood monocytes mimic endothelial progenitor cells, Stem Cells 24 (2006) 357–367.
[16] F. Timmermans, J. Plum, M.C. Yoder, D.A. Ingram, B. Vandekerckhove, J. Case, Endothelial progenitor cells: identity defined?, J. Cell. Mol. Med. 13 (2009) 87–102.
[17] J.M. Yoder, R.U. Aslam, N.J. Mantis, Evidence for widespread epithelial damage and coincident production of monocyte chemotactic protein 1 in a murine model of intestinal ricin intoxication, Infect. Immun. 75 (2007) 1745–1750.
[18] M. Lavergne, V. Vanneaux, C. Delmau, E. Gluckman, I. Rodde-Astier, J. Larghero, et al., Cord blood-circulating endothelial progenitors for treatment of vascular diseases, Cell Prolif. 44 (Suppl. 1) (2011) 44–47.
[19] A.C. Dudley, T. Udagawa, J.M. Melero-Martin, S.C. Shih, A. Curatolo, M.A. Moses, et al., Bone marrow is a reservoir for proangiogenic myelomonocytic cells but not endothelial cells in spontaneous tumors, Blood 116 (2010) 3367–3371.
[20] T. Asahara, Cell therapy and gene therapy using endothelial progenitor cells for vascular regeneration, Handb. Exp. Pharmacol. (2007) 181–194.
[21] C. Kalka, H. Masuda, T. Takahashi, W.M. Kalka-Moll, M. Silver, M. Kearney, et al., Transplantation of ex vivo expanded endothelial progenitor cells for therapeutic neovascularization, Proc. Natl. Acad. Sci. U.S.A. 97 (2000) 3422–3427.
[22] A. Kawamoto, H.C. Gwon, H. Iwaguro, J.I. Yamaguchi, S. Uchida, H. Masuda, et al., Therapeutic potential of ex vivo expanded endothelial progenitor cells for myocardial ischemia, Circulation 103 (2001) 634–637.
[23] G. Marsboom, S. Janssens, Endothelial progenitor cells: new perspectives and applications in cardiovascular therapies, Expert Rev. Cardiovasc. Ther. 6 (2008) 687–701.
[24] J.G. Roncalli, J. Tongers, M.A. Renault, D.W. Losordo, Endothelial progenitor cells in regenerative medicine and cancer: a decade of research, Trends Biotechnol. 26 (2008) 276–283.
[25] A.Z. Dudek, Endothelial lineage cell as a vehicle for systemic delivery of cancer gene therapy, Transl. Res. 156 (2010) 136–146.
[26] G. Collet, N. Lamerant-Fayel, M. Tertil, B. El Hafny-Rahbi, J. Stepniewski, A. Guichard, et al., Hypoxia-regulated overexpression of soluble VEGFR2 controls angiogenesis and inhibits tumor growth, Mol. Cancer Ther. 13 (2014) 165–178.
[27] A. Medvinsky, E. Dzierzak, Definitive hematopoiesis is autonomously initiated by the AGM region, Cell 86 (1996) 897–906.
[28] A. Cumano, I. Godin, Ontogeny of the hematopoietic system, Annu. Rev. Immunol. 25 (2007) 745–785.
[29] M.J. Chen, Y. Li, M.E. De Obaldia, Q. Yang, A.D. Yzaguirre, T. Yamada-Inagawa, et al., Erythroid/myeloid progenitors and hematopoietic stem cells originate from distinct populations of endothelial cells, Cell Stem Cell 9 (2011) 541–552.
[30] P.E. Young, S. Baumhueter, L.A. Lasky, The sialomucin CD34 is expressed on hematopoietic cells and blood vessels during murine development, Blood 85 (1995) 96–105.
[31] N. Kabrun, H.J. Buhring, K. Choi, A. Ullrich, W. Risau, G. Keller, Flk-1 expression defines a population of early embryonic hematopoietic precursors, Development 124 (1997) 2039–2048.
[32] J. Korhonen, A. Polvi, J. Partanen, K. Alitalo, The mouse tie receptor tyrosine kinase gene: expression during embryonic angiogenesis, Oncogene 9 (1994) 395–403.
[33] M. Ema, T. Yokomizo, A. Wakamatsu, T. Terunuma, M. Yamamoto, S. Takahashi, Primitive erythropoiesis from mesodermal precursors expressing VE-cadherin, PECAM-1, Tie2, endoglin, and CD34 in the mouse embryo, Blood 108 (2006) 4018–4024.
[34] N. Pfaff, N. Lachmann, M. Ackermann, S. Kohlscheen, C. Brendel, T. Maetzig, et al., A ubiquitous chromatin opening element prevents transgene silencing in pluripotent stem cells and their differentiated progeny, Stem Cells 31 (2013) 488–499.
[35] B.G. Pereira, S. Ligorio Fialho, C. Maria de Souza, G. Dantas Cassali, A. Silva-Cunha, Evaluation of the effects of thalidomide-loaded biodegradable devices in solid Ehrlich tumor, Biomed. Pharmacother. 67 (2013) 129–132.
[36] Y.I. Purwanti, C. Chen, D.H. Lam, C. Wu, J. Zeng, W. Fan, et al., Antitumor effects of CD40 ligand-expressing endothelial progenitor cells derived from human induced pluripotent stem cells in a metastatic breast cancer model, Stem Cells Transl. Med. 3 (2014) 923–935.
[37] R.K. Jain, An indirect way to tame cancer, Sci. Am. 310 (2014) 46–53.
[38] R.K. Jain, Antiangiogenesis strategies revisited: from starving tumors to alleviating hypoxia, Cancer Cell 26 (2014) 605–622.
[39] T. Korff, T. Krauss, H.G. Augustin, Three-dimensional spheroidal culture of cytotrophoblast cells mimics the phenotype and differentiation of cytotrophoblasts from normal and preeclamptic pregnancies, Exp. Cell Res. 297 (2004) 415–423.
[40] C. Kieda, B. El Hafny-Rahbi, G. Collet, N. Lamerant-Fayel, C. Grillon, A. Guichard, et al., Stable tumor vessel normalization with pO(2) increase and endothelial PTEN activation by inositol trispyrophosphate brings novel tumor treatment, J. Mol. Med. 91 (2013) 883–899.
[41] A. Bielawska-Pohl, S. Blesson, H. Benlalam, A. Trenado, P. Opolon, O. Bawa, et al., The anti-angiogenic activity of IL-12 is increased in iNOS–/– mice and involves NK cells, J. Mol. Med. 88 (2010) 775–784.
[42] S. Chouaib, C. Kieda, H. Benlalam, M.Z. Noman, F. Mami-Chouaib, C. Ruegg, Endothelial cells as key determinants of the tumor microenvironment: interaction with tumor cells, extracellular matrix and immune killer cells, Crit. Rev. Immunol. 30 (2010) 529–545.
[43] N. Bizouarne, V. Denis, A. Legrand, M. Monsigny, C. Kieda, A SV-40 immortalized murine endothelial cell line from peripheral lymph node high endothelium expresses a new alpha-L-fucose binding protein, Biol. Cell 79 (1993) 209–218.
[44] M. Paprocka, A. Krawczenko, D. Dus, A. Kantor, A. Carreau, C. Grillon, et al., CD133 positive progenitor endothelial cell lines from human cord blood, Cytometry A. 79 (2011) 594–602.
[45] J. Eggermann, S. Kliche, G. Jarmy, K. Hoffmann, U. Mayr-Beyrle, K.M. Debatin, et al., Endothelial progenitor cell culture and differentiation in vitro: a methodological comparison using human umbilical cord blood, Cardiovasc. Res. 58 (2003) 478–486.
[46] G.W. Basak, S. Yasukawa, A. Alfaro, S. Halligan, A.S. Srivastava, W.P. Min, et al., Human embryonic stem cells hemangioblast express HLA-antigens, J. Transl. Med. 7 (2009) 27.
[47] A. Matejuk, G. Collet, M. Nadim, C. Grillon, C. Kieda, MicroRNAs and tumor vasculature normalization: impact on anti-tumor immune response, Arch. Immunol. Ther. Exp. (Warsz) 61 (2013) 285–299.
[48] G. Collet, C. Grillon, M. Nadim, C. Kieda, Trojan horse at cellular level for tumor gene therapies, Gene 525 (2013) 208–216.
[49] S. Goel, D.G. Duda, L. Xu, L.L. Munn, Y. Boucher, D. Fukumura, et al., Normalization of the vasculature for treatment of cancer and other diseases, Physiol. Rev. 91 (2011) 1071–1121.
[50] Y. Sato, Persistent vascular normalization as an alternative goal of anti-angiogenic cancer therapy, Cancer Sci. 102 (2011) 1253–1256.
[51] K. Skrzypek, M. Tertil, S. Golda, M. Ciesla, K. Weglarczyk, G. Collet, et al., Interplay between heme oxygenase-1 and miR-378 affects non-small cell lung carcinoma growth, vascularization, and metastasis, Antioxid. Redox Signal. 19 (2013) 644–660.
[52] M. Vandamme, E. Robert, S. Lerondel, V. Sarron, D. Ries, S. Dozias, et al., ROS implication in a new antitumor strategy based on non-thermal plasma, Int. J. Cancer 130 (2012) 2185–2194.
[53] J. Stepniewski, N. Kachamakova-Trojanowska, D. Ogrocki, M. Szopa, M. Matlok, M. Beilharz, et al., Induced pluripotent stem cells as a model for diabetes investigation, Sci. Rep. 5 (2015) 8597.
[54] W. Yu, Z. Liu, S. An, J. Zhao, L. Xiao, Y. Gou, et al., The endothelial-mesenchymal transition (EndMT) and tissue regeneration, Curr. Stem Cell Res. Ther. 9 (2014) 196–204.